



HAL
open science

Release of internal molecular torque results in twists of Glaucocystis cellulose nanofibers

Yu Ogawa

► **To cite this version:**

Yu Ogawa. Release of internal molecular torque results in twists of Glaucocystis cellulose nanofibers. Carbohydrate Polymers, 2021, 251, pp.117102. 10.1016/j.carbpol.2020.117102 . hal-02977831

HAL Id: hal-02977831

<https://hal.science/hal-02977831>

Submitted on 14 Nov 2020

HAL is a multi-disciplinary open access archive for the deposit and dissemination of scientific research documents, whether they are published or not. The documents may come from teaching and research institutions in France or abroad, or from public or private research centers.

L'archive ouverte pluridisciplinaire **HAL**, est destinée au dépôt et à la diffusion de documents scientifiques de niveau recherche, publiés ou non, émanant des établissements d'enseignement et de recherche français ou étrangers, des laboratoires publics ou privés.

1 **Release of internal molecular torque results in twists of *Glaucocystis* cellulose**

2 **nanofibers**

3 Yu Ogawa

4 Univ. Grenoble Alpes. CNRS, CERMAV, 38000 Grenoble, France

5 Email address: yu.ogawa@cermav.cnrs.fr

6 Phone: +33 4 76 03 76 19; Fax: +33 4 76 54 72 03

7 ORCID: 0000-0003-0677-7913

8

9 **Abstract**

10 The cellulose of the green alga *Glaucocystis* consists of almost pure Ia crystalline phase
11 where the corresponding lattice b^* axis parameter lies perpendicular to the cell wall surface
12 in the multilamellar cell wall architecture, indicating that in this wall, cellulose is devoid of
13 longitudinal twist. In contrast, when isolated from *Glaucosytis* cell walls, the cellulose
14 microfibrils present a twisting behavior, which was investigated using electron microscopy
15 techniques. Sequential electron microdiffraction analyses obtained under frozen hydrated
16 conditions revealed that the cellulose microfibrils continuously right-hand twisted in the
17 vitreous ice layer. This observation implies that the twists of these nanofibers are intrinsic to
18 the cellulose molecule and not a result of the cell wall biogenesis process. Furthermore,
19 scaling with the fourth power of width based on the classic mechanics of solid, the twist
20 angle was in agreement with the reported values in higher plant celluloses, implying that the
21 twist arises from the balance between tendency of individual chains to twist and the structure
22 imposed by the crystal packing. The observed twist in isolated fibrils of *Glaucocystis*
23 indicates that one cannot assume the presence of cellulose twisting *in vivo* based on
24 observations of isolated cellulose nanoparticles, as microfibril can exist untwisted in the
25 original cell wall but become twisted when released from the wall.

26

27 **Keywords**; Cellulose I α ; Cryogenic transmission electron microscopy; Electron diffraction;

28 Twist; Nanofiber

29 1. Introduction

30 The morphology of cellulose nanoparticles, cellulose nanocrystals (CNC) and
31 cellulose nanofibers (CNF) have extensively been studied using various scattering and
32 microscopy techniques since this morphology strongly affects the final properties of materials
33 involving these nanoparticles (Elazzouzi-Hafraoui et al., 2008; Foster et al., 2018; Jakob,
34 Fratzl, & Tschegg, 1994; Mao et al., 2017). Alongside with the particle dimensions, fibrillar
35 twists of cellulose nanoparticles are among well studied morphological features of cellulose
36 at the nanometric scale (Hanley, Revol, Godbout, Gray, 1997; Usov et al., 2015; Nakai et al.,
37 2013; Hirai, Tsuji, & Horii, 1998). This is because the fibrillar twists are considered to reflect
38 the intrinsic chirality of cellulose and have high potential in high value-added applications
39 such as a nanosized chiral inducer (Kaushik et al., 2015; Majoinen et al., 2016). While the
40 uniaxial right-handed twists along the fiber axis of cellulose crystal have long been observed
41 under both electron and scanning probe microscopes, the quantitative analyses of this feature
42 have only recently been reported thanks to the methodological developments in the
43 microscopy techniques (Arcari et al., 2019; Bai et al., 2020; Ogawa, 2019). Computational
44 approaches such as force field simulations and quantum chemical calculations have also
45 contributed to understanding the nanoscale geometry of the twisting of cellulose crystals
46 (Conley, Godbout, Whitehead, & van de Ven, 2016; Dumitrică, 2020; Matthews et al., 2006;
47 Zhao et al., 2013).

48 Despite the efforts for characterizing the fibrillar twists of cellulose, many questions
49 about this twisting remain to be answered. The occurrence of the twists *in vivo* is such a
50 question. Some authors have speculated on the presence of the cellulose twisting in higher
51 plant cell walls (Fernandes et al., 2011; Park et al., 2013), but solid evidence is still lacking
52 for the twisting *in planta*. In contrast, it has been well demonstrated that such a fibrillar twist
53 does not exist in the cell walls of a series of green algae such as *Valonia*, *Oocystis*,

54 *Micrasterias* and *Glaucozystis* (Imai, Sugiyama, Itoh, & Horii, 1999; Kim, Herth, Vuong, &
55 Chanzy, 1996; Sugiyama, Chanzy, & Revol, 1994). In the cell wall of these green algae, the
56 cellulose microfibrils are organized into plywood-like multilamellar structures. Each lamella
57 consists of a parallel array of microfibrils and their orientation alternate between adjacent
58 lamellae (Itoh & Brown, 1984; Willison & Brown, 1978). Detailed X-ray and electron
59 diffraction studies revealed that the cellulose crystals show strict uniplanar orientations,
60 where either a^* or b^* reciprocal axis of the triclinic $I\alpha$ unit cell is always perpendicular to the
61 lamellar plane (Imai, Sugiyama, Itoh, & Horii, 1999; Sugiyama, Chanzy, & Revol, 1994).
62 Such a preferential orientation in the lateral plane of the crystals excludes the twisting of
63 cellulose crystals in these algal cell wall architectures. It is unclear, however, if the absence
64 of twist *in vivo* directly implies its absence in the isolated nanoparticle state.

65 In the present study, the nanoscale morphology of CNFs obtained from *Glaucozystis*
66 was investigated using a sequential electron microdiffraction method. The method was
67 developed in the previous report to investigate the twist geometry of tunicate CNCs that are
68 composed of pure cellulose $I\beta$ allomorph. In *Glaucozystis*, the cellulose microfibrils are
69 composed almost solely of the $I\alpha$ allomorph and not twisted in the cell wall (Imai, Sugiyama,
70 Itoh, & Horii, 1999; Nishiyama, Sugiyama, Chanzy, & Langan, 2003). Thus, it is an ideal
71 model specimen to investigate, on one hand, the effect of the isolation process and on the
72 other hand, the effect of the allomorphic structures on the nanoscale twist geometries. Based
73 on local crystallographic information obtained using the electron diffraction experiments, the
74 occurrence of fibrillar twist was observed, implying that the isolation process of cellulose
75 greatly altered the nanoscale geometry of cellulose crystals.

76

77 **2. Materials and methods**

78 **2.1. Sample preparation**

79 Cellulose microfibril suspensions from *Glaucozystis nostochinearum* were prepared
80 using sulfamic acid according to the method previously described by Briois et al (2013).
81 First, ghost cells of *G. nostochinearum* were prepared according to the method described by
82 Imai et al. (1999). These ghost cells were then dispersed into dimethylformamide (DMF) by
83 solvent exchange. The cells were transferred to 2 wt% sulfamic acid DMF solution and kept
84 overnight at 80 °C under mild agitation. The cells were then washed three times by
85 centrifugations in DMF and finally into the water where they spontaneously disrupted into
86 non-flocculating suspensions of individual cellulose microfibrils. The isolated cellulose
87 microfibrils will hereafter be referred to as CNFs.

88

89 **2.2 Transmission electron microscopy (TEM)**

90 All transmission electron microscopy was performed using a JEM-2100Plus (Jeol Ltd,
91 Japan). All the electron micrographs and diffraction patterns were recorded using a Gatan Rio
92 16 camera (Gatan Inc., USA) using the SerialEM program (Mastronarde, 2003). The sample
93 preparation and observation procedures for both conventional and cryogenic conditions were
94 described in a previous report (Ogawa, 2019).

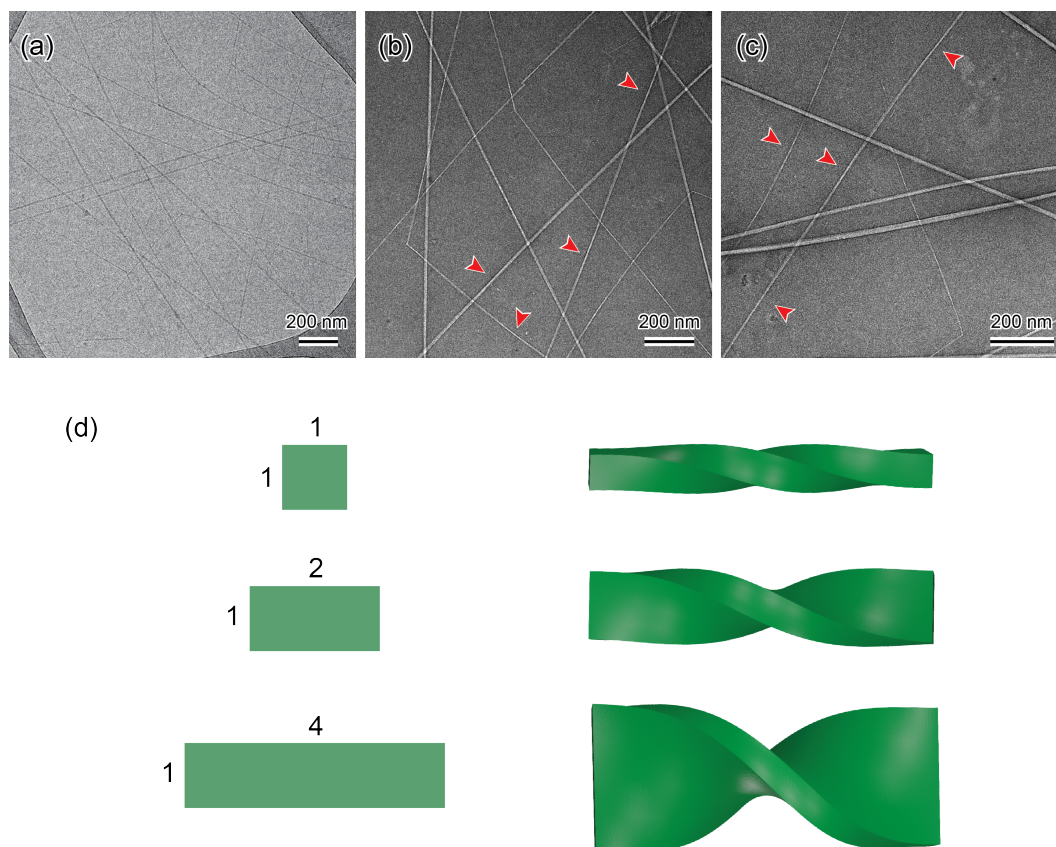
95

96 **3. Results**

97 **3.1. Morphology of *Glaucozystis* CNFs.**

98 Figure 1 shows cryogenic (Fig. 1a) and negatively stained (Figs. 1b and 1c) TEM
99 images of *Glaucozystis* CNFs. Individual CNFs were well dispersed and isolated after the
100 sulfamic acid treatment as reported previously (Briois et al., 2013). The sulfamic acid
101 treatment was chosen in this study as it provided long and straight nanofibers compared to the
102 short ones resulting from strong acid hydrolysis treatments, due to the less destructive nature
103 of the sulfamic treatment. As seen in Fig. 1c, the *Glaucozystis* CNFs show a wide distribution

104 of fibril width. The average width was estimated as 8.8 ± 3.0 nm from the negatively stained
105 images. There are slight changes in width along the fiber direction as indicated by
106 arrowheads in Figs. 1b and 1c, likely indicative of the presence of the fibrillar twist. While
107 they are more noticeable in the negatively stained images than in the cryoTEM counterparts,
108 this apparent width distribution is much less important compared to those in cellulose
109 microfibrils from other sources such as tunicate and bacteria (Elazzouzi-Hafraoui et al., 2008;
110 Usov et al., 2015). This is not surprising considering the difference in the cross-sectional
111 shapes of these cellulose microfibrils. The *Glaucocystis* microfibril has an approximately
112 square cross section while those of tunicate and bacterial cellulose microfibrils are more
113 elongated on one side of cross-sections than the other (Imai et al., 1999; Helbert, Nishiyama,
114 Okano, & Sugiyama 1998; Fang & Catchmark, 2014). As illustrated in Fig. 1d, a fiber with a
115 square cross section shows a smaller width modification along a 180° fibrillar twist compared
116 to ones presenting more elongated rectangular cross sections. This feature indicates a
117 potential drawback of conventional imaging and highlights the importance of using
118 crystallographic information to decipher the detailed twist geometry of cellulose crystals.
119



120

121 **Figure 1.** Morphology of *Glaucocystis* CNFs. (a) Diffraction contrast image of *Glaucocystis*
 122 CNFs in vitreous ice layer. (b, c) Negatively stained images of *Glaucocystis* CNFs dried on
 123 an amorphous carbon film. Arrowheads indicate apparent twist regions. (d) Schematic
 124 illustrations of width modification of twisted fibrils (right) with different cross-sectional
 125 shapes (left).

126

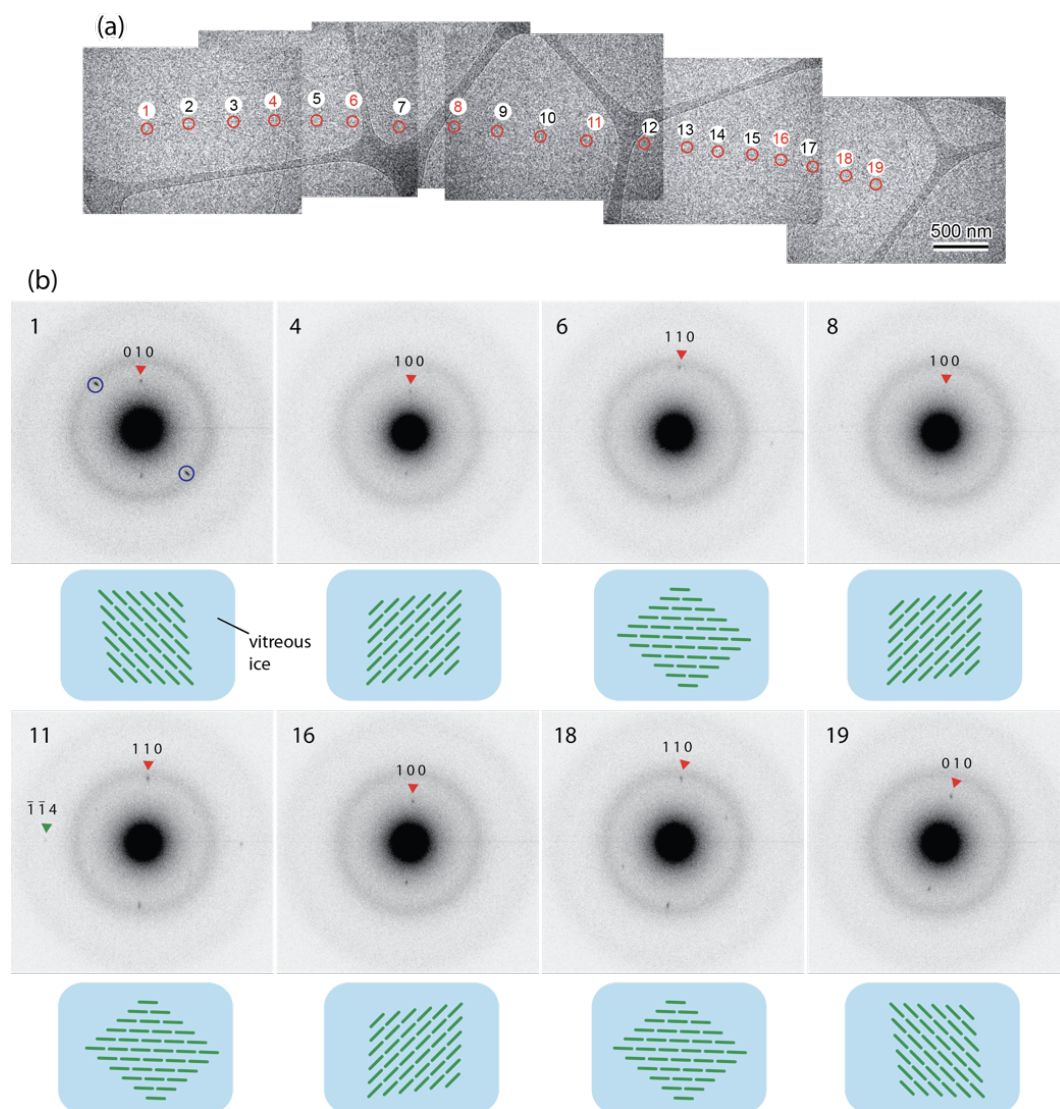
127 3.2. Twist geometry of *Glaucocystis* CNFs followed by electron microdiffraction

128 The twist geometry of *Glaucocystis* CNFs was then investigated using the electron
 129 microdiffraction technique using the method previously described (Ogawa, 2019). The
 130 electron microdiffraction allows obtaining local crystallographic information at a single
 131 nanoparticle level. Since the crystal structure of cellulose I α and the cross-sectional shape
 132 have been established in the literature (Imai et al., 1999; Nishiyama, Sugiyama, Chanzy, &
 133 Langan, 2003), one can determine the twist geometry of a CNF based on crystallographic

134 orientation obtained from two-dimensional microdiffraction data and the reported
135 information of the *Glaucozystis* cellulose crystal.

136 Figure 2 summarizes the microdiffraction analysis of a *Glaucozystis* CNF in vitreous
137 ice layer. The studied CNF is slightly curved as described in the literature (Imai et al., 1999).
138 There is no visible kink or defect in the studied area. The diffraction patterns were taken with
139 an interval of 2-300 nm and over a length of ca. 5.5 μm along the single CNF. As shown in
140 Fig. 2b, the diffraction patterns correspond to various projections depending on positions
141 along the CNF, indicating that it is rotated along its fiber axis. The patterns are successively
142 changing without showing identical diffraction patterns in consecutive positions. This implies
143 that the *Glaucozystis* CNF is continuously twisted in the vitreous ice layer and therefore in
144 the aqueous suspension. The twist rates of different areas along the single CNF are not
145 constant: $6.75^\circ/100$ nm between the positions 1 to 6, $8.2^\circ/100$ nm between 6 to 11, $8.4^\circ/100$
146 nm between 11 to 16, and $12^\circ/100$ nm between 16 to 19. The occurrence of the continuous
147 twisting in the aqueous suspension was also observed for the tunicate CNCs, and the reported
148 twist rates of the tunicate CNCs in the vitreous ice, $5\text{-}13^\circ/100$ nm, are comparable to those of
149 the *Glaucozystis* CNF in the present study (Ogawa, 2019).

150



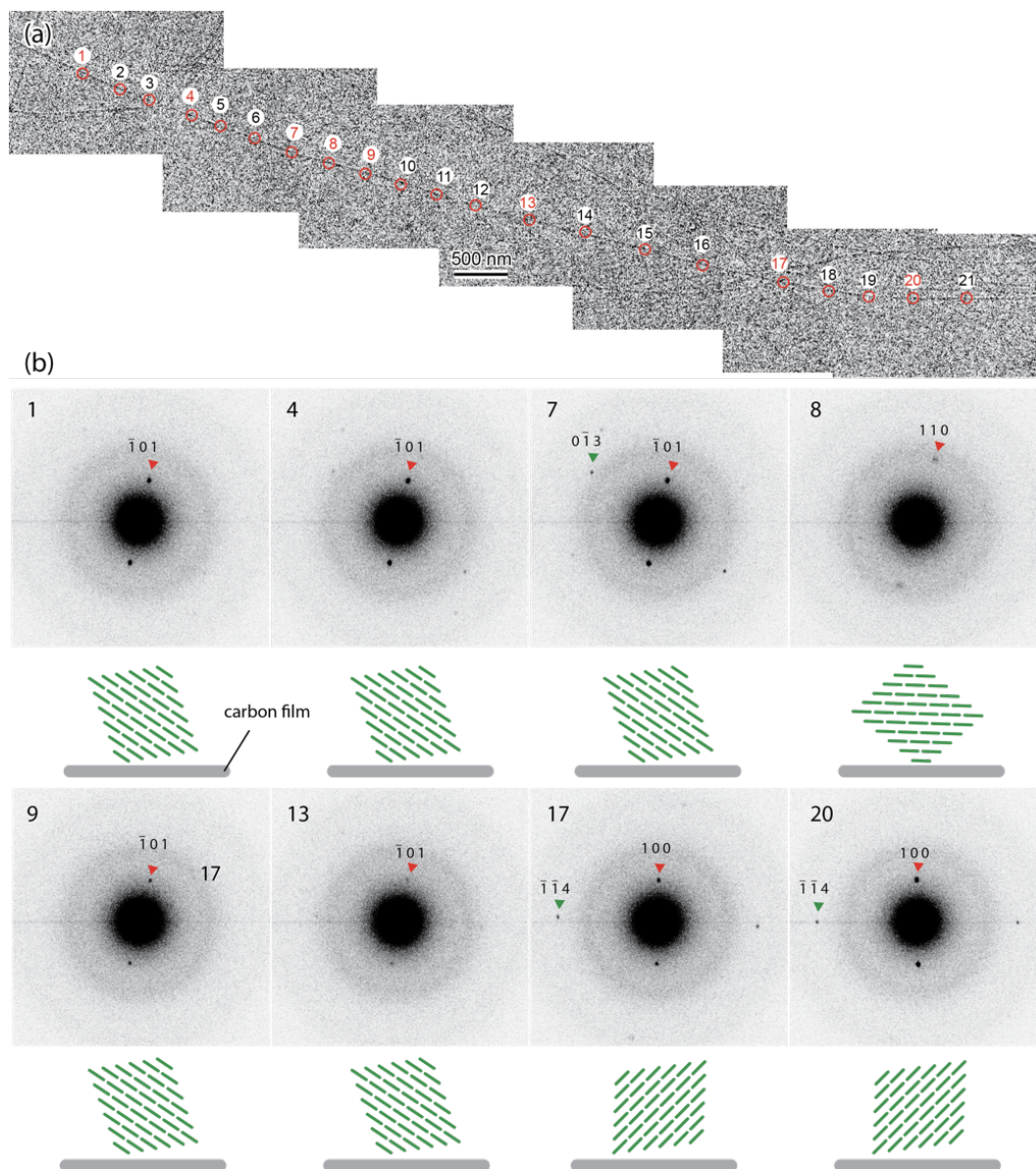
151

152 **Figure 2.** Electron microdiffraction analysis of the twist geometry of *Glaucocystis* CNF in
 153 vitreous ice layer. (a) Low-dose diffraction contrast image of studied *Glaucocystis* CNF.
 154 Circles indicate positions where diffraction patterns were taken. (c) Selected electron
 155 diffraction patterns taken from the CNF in (a) together with schematic illustrations of cross-
 156 sectional orientation at each position. In these schemes electrons are irradiating from the top
 157 side. Circled diffraction spots in the pattern 1 are not from the studied CNF but from another
 158 CNF.

159

160 A similar electron microdiffraction analysis was carried out with a *Glaucocystis* CNF
 161 dried on an amorphous carbon film. The studied CNF was roughly straight without any

162 visible kinks or defected area. The diffraction patterns were taken with an interval of ca. 300
163 nm and with an overall length of ca. 6 μm along the single CNF. As in the data set taken
164 under cryo condition (Fig. 2b), the diffraction patterns show different projections of cellulose
165 I α crystal depending on the acquisition positions, indicative of the presence of fibrillar twist
166 (Fig. 3b). Unlike the continuous twisting of the CNF in the vitreous ice layer, the dry
167 *Glaucozystis* CNF shows a discontinuous twist geometry. The diffraction patterns obtained at
168 the positions from 1 to 7 show the identical projection containing the -1 0 1 reciprocal vector,
169 pointing a presence of a flat segment over about 2 μm . A similar flat segment extends
170 between the positions from 9 to 13. A different projection containing 1 1 0 reciprocal vector
171 is observed at the position 8 which locates between two flat segments. This means that the
172 CNF is twisted sharply by 180° in the length of about 600 nm between the positions 7 and 9.
173 The alternate occurrence of flat segments and a sharp twist region is clearly different from the
174 continuous twisting of the CNF in the vitreous ice. The twist geometry of *Glaucozystis* CNFs
175 is thus altered upon drying on the flat carbon substrate. A similar alteration of the twist
176 geometry upon drying was observed for the tunicate CNCs and likely a common
177 phenomenon for isolated cellulose nanoparticles (Ogawa, 2019).



178

179 **Figure 3.** Electron microdiffraction analysis of the twist geometry of *Glaucocystis* CNF dried

180 on an amorphous carbon film. (a) Low-dose diffraction contrast image of studied

181 *Glaucocystis* CNF. Circles indicate positions where diffraction patterns were taken. (c)

182 Selected electron diffraction patterns taken from the CNF in (a) together with schematic

183 illustrations of cross-sectional orientation at each position. In these schemes electrons are

184 irradiating from the top side.

185

186 **4. Discussion**

187 The present electron microdiffraction analyses have clearly demonstrated that when
188 extracted from their cell wall the individual *Glaucocystis* CNFs are twisted in both the
189 aqueous and the dry conditions. As abovementioned their twists are less visible compared to
190 those of other cellulose nanoparticles likely due to their square cross sections (Fig. 1). The
191 electron diffraction-based analysis is thus essential to reveal the detailed twist geometry of
192 the *Glaucocystis* CNFs.

193 Such fibrillar twists are absent in the cellulose microfibrils in the *Glaucocystis* cell
194 wall as aforementioned the introduction. This difference in the fibril morphologies *in vivo*
195 and in the isolated state indicates that the fibrillar twist is introduced during the isolation
196 process, where the occurrence of the twists suggests that the twisting arises as a consequence
197 of relaxation from mechanical constraints pre-existing in the cell wall. Such constraints can
198 originate from various reasons from biosynthesis mechanisms of cellulose microfibrils and
199 their tight packing in the lamellar structure, to surface interactions of the microfibrils with
200 other materials in the cell wall. In the cellulose biosynthesis the cellulose microfibrils are
201 secreted from a membrane-bound protein complex, namely cellulose synthase complex
202 (CSC) (Turner & Kumar, 2018). The CSC moves on the plasma membrane plane as it
203 deposits a microfibril which is anchored on the cell surface (Paredes, Somerville, & Ehrhardt,
204 2006). This situation imposes a deposition of microfibrils laid flat on the cell surface as
205 previously proposed. The tight packing of microfibrils with matrix materials in the lamella
206 structure would not allow a structural relaxation of the cellulose crystal but further
207 immobilize the flat morphology even when the deposited cellulose layer is detached from the
208 plasma membrane. The removal of the matrix material and the disruption of the cell wall
209 during the microfibril isolation in aqueous environment induce its relaxation with the likely
210 consequence of the twist morphology. While many biological and structural aspects of
211 cellulose biosynthesis are still elusive in both algal and higher plant systems, one should

212 expect a similar geometrical constraint in secretion of cellulose microfibrils in any cellulosic
213 systems. The process-induced twist of the CNFs shown in this study underlines the fact that it
214 is dangerous to assume the occurrence of cellulose twisting *in planta* simply based on
215 observations of twists of isolated nanoparticles.

216 The *Glaucozystis* cellulose studied in this study is composed of almost pure Ia
217 allomorph in contrast to the pure I β tunicate cellulose studied in the previous report (Belton,
218 Tanner, Cartier, & Chanzy, 1989). Despite having different allomorphs, the two specimens,
219 *Glaucozystis* CNF and tunicate CNC show similar continuous twist geometries with twisting
220 rates of the same order of magnitude in vitreous ice layers. While the comparison is yet to be
221 systematically made among cellulose crystals with various Ia/I β ratios, this comparison
222 between two extreme examples suggest that the allomorphic structure is not a dominant
223 factor that controls the fibrillar twist geometry of native cellulose crystals.

224 In contrast, the fibril width has a significant effect on the twist morphology. Based on
225 the twist rate and the fibril width measured in the current analysis, one can estimate an
226 applied torque to the studied CNF. In classic solid mechanics, a torque, T , applied to a
227 straight bar is given as

$$228 \quad T = GJ\theta/L$$

229 , where G is a shear modulus, J is torsion constant, θ is a twist angle and L is a length of the
230 bar. The torsion constant is a function of cross-sectional shape and one for a square cross
231 section bar is given as

$$232 \quad J_{square} = 0.1406 a^4$$

233 , where a is the square side length. The shear modulus G_{ab} of the cellulose crystal was
234 estimated as 3.4 GPa based on a force field simulation (Chen, Ogawa, Nishiyama, Ismail,
235 Mazeau, 2016). The fibril width of the CNF in Fig. 2a is ca. 10 nm and a twist rate of 8°/100
236 nm is used as a representative value, which gives a torque T of 6.67 nN·nm. The cross section

237 of 10 nm×10 nm of an Ia crystal contains 15 (along *a*-axis) ×17 (along *b*-axis) = 255
 238 molecular chains, so the torque per molecular chain is 26 pN·nm. Based on this torque value,
 239 a twist pitch, a fibril length for a 180° turn can be estimated for a cellulose crystal with a
 240 given cross section. The higher plant cellulose microfibrils are proposed to have a round
 241 cross section composed of 18 molecular chains (Jarvis, 2017; Nixon et al., 2016). The torsion
 242 constant of a bar with a round cross section is given as

$$243 \quad J_{round} = \pi d^4/32$$

244 where *d* is a fibril diameter. The twist pitch is estimated as 137 nm for a cellulose crystal with
 245 a round cross section composed of 18 molecular chains with *d* = 2.8 nm. While the
 246 dimensions of a hexagonal cross section, another common cross-sectional model, can be
 247 considered approximately the same with the round cross section, a rectangular cross section,
 248 (3 × 6 chains, *a* = 2.8 nm, *b* = 2 nm) gives a different estimation of the twist pitch. A torsion
 249 constant of a bar with a rectangular cross section is given as

$$250 \quad J_{rectangular} = ab^3 \left[\frac{16}{3} - 3.36 \frac{b}{a} \left(1 - \frac{b^4}{12a^4} \right) \right].$$

251 Thus, the estimated twist pitch for this fibril with the rectangular cross section is 95 nm. This
 252 value is 44% shorter than that of the round cross section, highlighting the importance of the
 253 cross-sectional shape on the twist geometry of cellulose crystals. These estimated pitch
 254 values agree with the values based on AFM observations of softwood CNFs (90-140 nm)
 255 even though the charge effect is not considered in this current estimation (Arcari et al., 2019).
 256 This agreement indicates that the molecular torque is intrinsic to the cellulose molecule and
 257 constant regardless of biological origin of cellulose crystals. It also implies that the twist
 258 geometry of the isolated cellulose crystals is not depending on their biological origins but on
 259 their torsion constant determined by their cross-sectional shapes. Since the torque is intrinsic
 260 to the molecule and thus pre-exists in untwisted cellulose microfibrils in a constrained cell

261 wall architecture, a gentle isolation process without strong mechanical homogenization is
262 enough to induce the fibrillar twists to cellulose crystals.

263 The twist pitch predicted by theoretical methods shows a large diversity depending on
264 the used methods: for a fibril model with the same square cross section composed of 36
265 molecular chains with $a = 3.6$ nm, a force field simulation estimates the pitch as 150 nm,
266 while a density-functional based tight-binding calculation predicts it as 380 nm (Dumitrică,
267 2020; Zhao et al., 2013). The corresponding twist pitch is estimated as 268 nm based on the
268 torque calculated from the current observation. The validity of the theoretical predictions of
269 the twist geometry has to be confirmed with quantitative experimental observations that have
270 recently become more available.

271

272 **5. Conclusion**

273 A sequential electron microdiffraction method was applied to the *Glaucozystis* CNFs
274 to investigate the effects of the allomorphic structures and the isolation process on the twist
275 geometry of the cellulose crystals. The microdiffraction method was essential for this
276 investigation since the fibrillar twists of *Glaucozystis* CNFs were barely visible due to their
277 square cross-sectional shape, hindering an imaging-based characterization. The series of
278 electron diffraction patterns obtained under cryogenic condition revealed the presence of the
279 continuous twisting of *Glaucozystis* CNF composed of almost pure Ia crystal in vitreous ice
280 layer. In a similar manner with the previously observed tunicate CNCs, this regular twist was
281 altered to discontinuous sharp twists and flat segments upon drying on flat carbon substrates.
282 Since the cellulose microfibrils are untwisted in the *Glaucozystis* cell wall, this twisting is
283 thus a consequence of the nanofiber isolation treatment. Our study sheds light into the
284 discussion on the presence of the fibrillar twists of cellulose crystals *in vivo*. Further

285 structural investigations are needed to elucidate whether such twists exist in other algal and
286 higher plant cell walls.

287 The torque applied to the cellulose crystal was calculated based on the current
288 observation, allowing estimating the twist pitch of crystals of different cross-sectional
289 morphologies. The estimated pitch value for a thinner crystal is in good agreement with the
290 experimental observations of softwood CNFs. This indicates a strong dependence of the twist
291 geometry of isolated cellulose crystals on the cross-sectional sizes and shapes.

292

293 **Acknowledgement**

294 I thank Dr Yoshiharu Nishiyama, Dr Karim Mazeau, Dr Henri Chanzy, and Mr Pierre Sailer
295 for their help during the writing of this article. I acknowledge the NanoBio-ICMG platform
296 (FR 2607) for granting access to the electron microscopy facility and Glyco@Alps (ANR-15-
297 IDEX-02) for financial support.

298

299 **Reference**

300 Arcari, M., Zuccarella, E., Axelrod, R., Adamcik, J., Sánchez-Ferrer, A., Mezzenga, R., &
301 Nyström, G. (2019). Nanostructural properties and twist periodicity of cellulose
302 nanofibrils with variable charge density. *Biomacromolecules*, 20(3), 1288-1296.

303 Bai, L., Kämäräinen, T., Xiang, W., Majoinen, J., Seitsonen, J., Grande, R., Huan, S., Liu, L.,
304 Fan, Y., & Rojas, O. J. (2020). Chirality from Cryo-Electron Tomograms of
305 Nanocrystals Obtained by Lateral Disassembly and Surface Etching of Never-Dried
306 Chitin. *ACS Nano*, 14(6) 6921-6930.

307 Belton, P. S., Tanner, S. F., Cartier, N., & Chanzy, H. (1989). High-resolution solid-state
308 carbon-13 nuclear magnetic resonance spectroscopy of tunicin, an animal cellulose.
309 *Macromolecules*, 22(4), 1615-1617.

310 Briois, B., Saito, T., Pétrier, C., Putaux, J. L., Nishiyama, Y., Heux, L., & Molina-Boisseau,
311 S. (2013). I α \rightarrow I β transition of cellulose under ultrasonic radiation. *Cellulose*, 20(2),
312 597-603.

313 Chen, P., Ogawa, Y., Nishiyama, Y., Ismail, A. E., & Mazeau, K. (2016). Linear, non-linear
314 and plastic bending deformation of cellulose nanocrystals. *Physical Chemistry*
315 *Chemical Physics*, 18(29), 19880-19887.

316 Conley, K., Godbout, L., Whitehead, M. T., & van de Ven, T. G. (2016). Origin of the twist
317 of cellulosic materials. *Carbohydrate polymers*, 135, 285-299.

318 Dumitrică, T. (2020). Intrinsic twist in I β cellulose microfibrils by tight-binding objective
319 boundary calculations. *Carbohydrate Polymers*, 230, 115624.

320 Elazzouzi-Hafraoui, S., Nishiyama, Y., Putaux, J. L., Heux, L., Dubreuil, F., & Rochas, C.
321 (2008). The shape and size distribution of crystalline nanoparticles prepared by acid
322 hydrolysis of native cellulose. *Biomacromolecules*, 9(1), 57-65.

323 Fang, L., & Catchmark, J. M. (2014). Characterization of water-soluble exopolysaccharides
324 from *Gluconacetobacter xylinus* and their impacts on bacterial cellulose
325 crystallization and ribbon assembly. *Cellulose*, 21(6), 3965-3978.

326 Fernandes, A. N., Thomas, L. H., Altaner, C. M., Callow, P., Forsyth, V. T., Apperley, D. C.,
327 Kennedy, C. J., & Jarvis, M. C. (2011). Nanostructure of cellulose microfibrils in
328 spruce wood. *Proceedings of the National Academy of Sciences*, 108(47), E1195-
329 E1203.

330 Foster, E. J., Moon, R. J., Agarwal, U. P., Bortner, M. J., Bras, J., Camarero-Espinosa, S., et
331 al. (2018). Current characterization methods for cellulose nanomaterials. *Chemical*
332 *Society Reviews*, 47(8), 2609-2679.

333 Hanley, S. J., Revol, J. F., Godbout, L., & Gray, D. G. (1997). Atomic force microscopy and
334 transmission electron microscopy of cellulose from *Micrasterias denticulata*;
335 evidence for a chiral helical microfibril twist. *Cellulose*, 4(3), 209.

336 Helbert, W., Nishiyama, Y., Okano, T., & Sugiyama, J. (1998). Molecular imaging of
337 *Halocynthia papillosa* cellulose. *Journal of Structural Biology*, 124(1), 42-50.

338 Hirai, A., Tsuji, M., & Horii, F. (1998). Helical sense of ribbon assemblies and splayed
339 microfibrils of bacterial cellulose. *Sen'i Gakkaishi*, 54(10), 506-510.

340 Kim, N. H., Herth, W., Vuong, R., & Chanzy, H. (1996). The cellulose system in the cell
341 wall of *Micrasterias*. *Journal of Structural Biology*, 117(3), 195-203.

342 Imai, T., Sugiyama, J., Itoh, T., & Horii, F. (1999). Almost pure I α cellulose in the cell wall
343 of *Glaucocystis*. *Journal of Structural Biology*, 127(3), 248-257.

344 Itoh, T., & Brown, R. M. (1984). The assembly of cellulose microfibrils in *Valonia*
345 *macrophysa* Kütz. *Planta*, 160(4), 372-381.

346 Jakob, H. F., Fratzl, P., & Tschegg, S. E. (1994). Size and arrangement of elementary
347 cellulose fibrils in wood cells: a small-angle X-ray scattering study of *Picea*
348 *abies*. *Journal of Structural Biology*, 113(1), 13-22.

349 Jarvis, M. C. (2018). Structure of native cellulose microfibrils, the starting point for
350 nanocellulose manufacture. *Philosophical Transactions of the Royal Society A:*
351 *Mathematical, Physical and Engineering Sciences*, 376(2112), 20170045.

352 Kaushik, M., Basu, K., Benoit, C., Cirtiu, C. M., Vali, H., & Moores, A. (2015). Cellulose
353 nanocrystals as chiral inducers: enantioselective catalysis and transmission electron
354 microscopy 3D characterization. *Journal of the American Chemical Society*, 137(19),
355 6124-6127.

356 Mao, Y., Liu, K., Zhan, C., Geng, L., Chu, B., & Hsiao, B. S. (2017). Characterization of
357 nanocellulose using small-angle neutron, X-ray, and dynamic light scattering
358 techniques. *The Journal of Physical Chemistry B*, *121*(6), 1340-1351.

359 Majoinen, J., Hassinen, J., Haataja, J. S., Rekola, H. T., Kontturi, E., Kostianen, M. A., Ras,
360 R. H. A., Törmä, P., & Ikkala, O. (2016). Chiral plasmonics using twisting along
361 cellulose nanocrystals as a template for gold nanoparticles. *Advanced*
362 *Materials*, *28*(26), 5262-5267.

363 Mastrorarde, D. N. (2003). SerialEM: a program for automated tilt series acquisition on
364 Tecnai microscopes using prediction of specimen position. *Microscopy and*
365 *Microanalysis*, *9*(S02), 1182-1183.

366 Matthews, J. F., Skopec, C. E., Mason, P. E., Zuccato, P., Torget, R. W., Sugiyama, J.,
367 Himmel, M. E., & Brady, J. W. (2006). Computer simulation studies of
368 microcrystalline cellulose I β . *Carbohydrate research*, *341*(1), 138-152.

369 Nakai, T., Sugano, Y., Shoda, M., Sakakibara, H., Oiwa, K., Tuzi, S., Imai, T., Sugiyama, J.,
370 Takeuchi, M., Yamauchi, D., & Mineyuki, Y. (2013). Formation of highly twisted
371 ribbons in a carboxymethylcellulase gene-disrupted strain of a cellulose-producing
372 bacterium. *Journal of Bacteriology*, *195*(5), 958-964.

373 Nishiyama, Y., Sugiyama, J., Chanzy, H., & Langan, P. (2003). Crystal structure and
374 hydrogen bonding system in cellulose I α from synchrotron X-ray and neutron fiber
375 diffraction. *Journal of the American Chemical Society*, *125*(47), 14300-14306.

376 Nixon, B. T., Mansouri, K., Singh, A., Du, J., Davis, J. K., Lee, J. G., Slabaugh, E.,
377 Vandavasi, V. G., O'Neill, H., Roberts, E. M., Roberts, A. W., Yingling, Y. G., &
378 Haigler, C. H. (2016). Comparative structural and computational analysis supports
379 eighteen cellulose synthases in the plant cellulose synthesis complex. *Scientific*
380 *Reports*, *6*(1), 28696.

381 Ogawa, Y. (2019). Electron microdiffraction reveals the nanoscale twist geometry of
382 cellulose nanocrystals. *Nanoscale*, 11(45), 21767-21774.

383 Park, Y. B., Lee, C. M., Koo, B. W., Park, S., Cosgrove, D. J., & Kim, S. H. (2013).
384 Monitoring meso-scale ordering of cellulose in intact plant cell walls using sum
385 frequency generation spectroscopy. *Plant Physiology*, 163(2), 907-913.

386 Paredez, A. R., Somerville, C. R., & Ehrhardt, D. W. (2006). Visualization of cellulose
387 synthase demonstrates functional association with microtubules. *Science*, 312(5779),
388 1491-1495.

389 Sugiyama, J., Chanzy, H., & Revol, J. F. (1994). On the polarity of cellulose in the cell wall
390 of *Valonia*. *Planta*, 193(2), 260-265.

391 Turner, S., & Kumar, M. (2018). Cellulose synthase complex organization and cellulose
392 microfibril structure. *Philosophical Transactions of the Royal Society A:
393 Mathematical, Physical and Engineering Sciences*, 376(2112), 20170048.

394 Usov, I., Nyström, G., Adamcik, J., Handschin, S., Schütz, C., Fall, A., Bergström, L., &
395 Mezzenga, R. (2015). Understanding nanocellulose chirality and structure–properties
396 relationship at the single fibril level. *Nature Communications*, 6(1), 1-11.

397 Willison, J. H., & Brown Jr, R. M. (1978). Cell wall structure and deposition in
398 *Glaucocystis*. *The Journal of Cell Biology*, 77(1), 103-119.

399 Zhao, Z., Shklyaev, O. E., Nili, A., Mohamed, M. N. A., Kubicki, J. D., Crespi, V. H., &
400 Zhong, L. (2013). Cellulose microfibril twist, mechanics, and implication for
401 cellulose biosynthesis. *The Journal of Physical Chemistry A*, 117(12), 2580-2589.